Flight Testing Total Energy Control Autopilot Functionalities for High Altitude Aircraft

Christian Weiser* and Gertjan Looye†
German Aerospace Center (DLR), 82234 Weßling, Germany

Daniel Ossmann‡
Munich University of Applied Sciences HM, 80335 Munich, Germany

In this paper the design and flight testing of a Total Energy Control System (TECS) autopilot for a High Altitude Long Endurance (HALE) aircraft is presented. Autopilot control for HALE aircraft is a well-fitting application for the TECS control strategy, as this enables energy-efficient, decoupled airspeed and flight path control with explicitly handling thrust limitation. To achieve a realistic validation of the controller before moving towards the integration on the HALE platform, the flight testing is carried out on a Cessna Citation passenger aircraft. It has been proven that the adjustments required to implement the control laws on the Cessna Citation passenger aircraft are minimal. This indicates that the Cessna Citation aircraft serves excellently as a hardware platform and can be utilized for the validation of flight control code integration and functionality. The results of the flight test are discussed, and insights gleaned for the future integration of TECS on the HALE aircraft are provided.

Nomenclature

$\dot{D}$	=	energy distribution rate
$\dot{E}$	=	energy rate
g	=	gravitational constant
h	=	altitude
K	=	controller gain
m	=	mass
$N1$	=	engine rotational speed (power setting)
V_{tas}	=	true airspeed
T	=	thrust
kin	=	index for kinetic energy
pot	=	index for potential energy
s	=	index for specific energy
α	=	angle of attack
γ	=	flight path angle
Θ	=	pitch attitude
ξ	=	aileron deflection
η	=	elevator deflection
ζ	=	rudder deflection

*Research Associate, christian.weiser@dlr.de, AIAA Member
†Head of Department, gertjan.looye@dlr.de
‡Professor, daniel.ossmann@hm.edu, AIAA Senior Member

I. Introduction

High Altitude Long Endurance (HALE) aircraft are designed for operation at altitudes of 18 - 25 km in the stratosphere. The mission scenarios for these aircraft are similar to those of satellites, requiring the platform to stay airborne in the stratosphere for various durations, ranging from several days to multiple months. In addition to the constant operation at these high altitudes, the ascent and descent phases of the flight cycle are critical, during which the aircraft is subjected to disturbances, for example turbulence. Maintaining flight using solar energy necessitates extremely lightweight structures along with a flight control system that safely guides the aircraft with a minimal amount of propulsion energy. One type of flight control architecture suited for this task is the well-known Total Energy Control System (TECS) architecture [1]. This architecture can successfully minimize the amount of specific excess energy added, as the total energy rate is one of the control variables.

Fig. 1 Exemplary High Altitude Long Endurance (HALE) aircraft illustration (Copyright: DLR).

The aircraft for which the TECS autopilot design shall be verified is the German Aerospace Center (DLR)'s HALE platform 'HAPomega' [2]. An artistic representation of this HALE aircraft is depicted in Fig. 1. An initial flight control design [3, 4] is already publicly available, which includes a comparison between the TECS system and a robust control-based autopilot [5]. The novelty of this paper lies in the direct application of the TECS autopilot, which is designed specifically for the HALE platform, and testing it in flight on the CS25 Cessna Citation aircraft of TU Delft. The purpose of the presented flight test campaign is the validation of the implementation and the functionalities of the designed TECS autopilot as well as the validation of the code generation tool-chain. Since the actual flight hardware of the HALE platform isn't currently available and is expected in the future, the Cessna Citation passenger aircraft enables the integration and flight testing of the control algorithms already at this early development stage. This aircraft has been extensively utilized in several previous flight testing campaigns and has proven its reliability during the development cycle of various flight control system developments. Past flight tests have included, for example, Linear Parameter Varying (LPV) and Incremental non-linear dynamic inversion (INDI) inner loop control laws [6–10], resulting in a robust and well-known code generation and integration tool-chain. This implies that the Cessna Citation aircraft serves successfully as a hardware platform and can be utilized for validating the flight control code integration and functionality. Furthermore, this paper demonstrates that minimal adjustments are needed to implement the control laws on the Cessna Citation passenger aircraft. Consequently, we can assume the validity of the presented flight tests for the TECS control laws applied to the HALE aircraft.

The initial part of the paper introduces the flight control architecture and provides an overview of the test framework. Subsequently, the TECS algorithm, as described in [11], is presented. This is followed by the presentation of modifications and the tested design of the TECS controller. Afterwards, the flight test aircraft and test results are introduced. Finally, an analysis and discussion of the results is given, focusing on the implications for the usage of the flight control algorithms on the HALE aircraft.

II. TECS Flight Control System

The chosen flight control architecture is depicted in Fig. 2, which has already been presented in [3]. This paper focuses on the development of the outer loop TECS control laws for the HALE aircraft, highlighted in orange in Fig. 2. The inputs for the longitudinal autopilot control law are the reference flight path angle γ_{cmd}, the commanded altitude h_{cmd}, and the airspeed command $V_{\text{cas, cmd}}$. The autopilot for the longitudinal aircraft dynamics generates the thrust (δ_T) and pitch attitude command ($\Delta\Theta_{\text{cmd}}$) as outputs. In the case of the actual HALE aircraft design, the pitch attitude command is fed to the baseline pitch controller. This baseline controller is a rate-command, attitude-hold controller based on gain-scheduled proportional and integral feedback, see [3] for details. For the flight experiments on the Cessna Citation, however, an INDI inner loop controller [8, 12] and an LPV controller [7] are available. Both have the same input-output interface as the HALE baseline controller, i.e., receiving pitch angle commands from the autopilot and generating the elevator deflection angle δ_e. Also, both have been analyzed in previous campaigns and showed good tracking performance for the Cessna Citation aircraft and could cope well with the aircraft's dynamics and limitations. For the tests presented in this paper, the INDI controller has been selected.

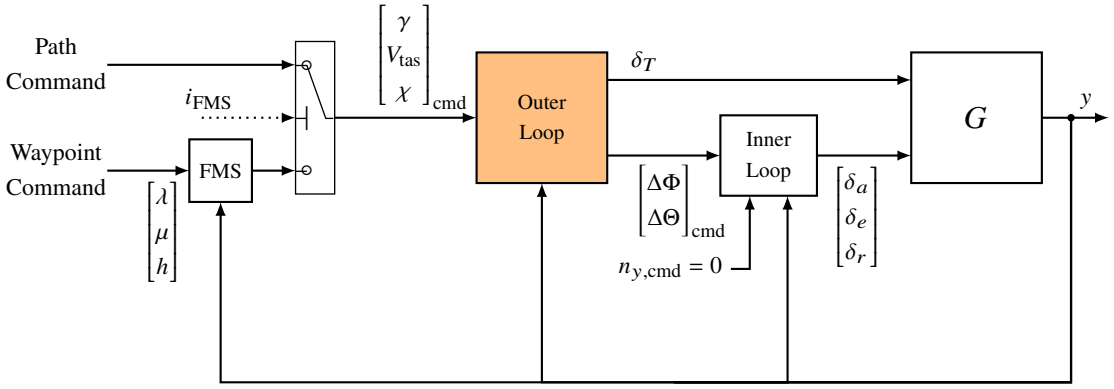

Fig. 2 Architecture of the HALE & research flight control system.

The flight dynamics of the Cessna Citation, denoted as G in Fig. 2, is based on the DASMAT aircraft model [13], which has been implemented and verified throughout previous flight test campaigns, e.g. [6, 9, 10].

A. Total Energy Control System

A longitudinal autopilot concept, which offers decoupling of airspeed and flight path angle (FPA), is the Total Energy Control System. The control strategy was initially introduced in the early 80s by A. Lambregts [1] and subsequently flight-tested by NASA and Boeing [14]. It has been applied in previous HALE design projects as well [15] and is a promising approach for the energy efficient combined speed and flight path control for HALE aircraft. Furthermore, it already includes modes for the rapid switching from standard speed / flight path decoupling to speed priority which is needed in case of thrust saturation. In this section, the TECS design philosophy as well as the adaptions made for both, the HALE and Cessna Citation, are presented.

The TECS control law is based on the principle of the overall energy of an aircraft, i.e., $E = E_{\text{pot}} + E_{\text{kin}}$. With the small angle approximation $\dot{h} \simeq V\gamma$, the derivative of the total energy equation is given by

$$\dot{E} = m\,g\,\dot{h} + m\,V\,\dot{V} \simeq m\,g\,V\left(\gamma + \frac{\dot{V}}{g}\right). \tag{1}$$

Assuming that the increase in drag ΔD is slight compared to the thrust increase ΔT in (2), an energy change $\dot{E}$ can directly be related to a thrust command T_{cmd}. Introducing the specific total energy rate $\dot{E}_S = \dot{E}/(mgV)$ and considering the control errors in FPA and equivalent airspeed result in

$$\begin{aligned} \Delta\dot{E}_S &= (\gamma_{\text{cmd}} - \gamma) + (\dot{V}_{\text{cmd}} - \dot{V})/g \\ &= (\Delta T_{\text{cmd}} - \Delta D)/(m\,g) \simeq \Delta T_{\text{cmd}}/(m\,g), \end{aligned} \tag{2}$$

describing the commanded specific energy rate change. Finally, a proportional-integral (PI) control law for the thrust

can be defined by

$$\frac{T_{\text{cmd}}}{mg} = K_{TI} \int \Delta \dot{E}_S dt - K_{TP} \dot{E}_S. \tag{3}$$

To derive the second command signal $\delta\Theta_{\text{cmd}}$, the specific energy distribution $\dot{D}_s$ between kinematic and potential energy rate is simply defined by the difference of the two energy types,

$$\dot{D}_S = -E_{\text{S,pot}} + E_{\text{S,kin}} = -\gamma + \frac{\dot{V}}{g}. \tag{4}$$

The specific energy distribution can be fed back due to the substitution in (4) by the measurements γ and $\dot{V}$. To enable a feedback loop, the measurements are subtracted from their demands

$$\Delta \dot{D}_S = \dot{D}_{S,\text{cmd}} - \dot{D}_S = -(\gamma_{\text{cmd}} - \gamma) + \frac{(\dot{V}_{\text{cmd}} - \dot{V})}{g}. \tag{5}$$

Finally, using the assumption that the commanded energy distribution rate is proportional to the commanded pitch attitude [11], i.e., $\Delta \dot{D}_S \propto \Delta\Theta_{\text{cmd}}$, the outer loop control law

$$\Delta\Theta_{\text{cmd}} \propto K_{DI} \int \Delta \dot{D}_S dt - K_{DP} \dot{D}_S \tag{6}$$

can be derived.

B. Implementation

The block diagram of the TECS described in Sec. II.A is shown in Fig. 3. Compared to the equations in Sec. II.A, however, it can be noted that the proportional gains only use the feedback and not the error path. This has been explained in [1] with introducing less overshoot (without influencing the stability characteristics). The TECS structure depicted in Fig. 3 is used for the HALE as well as the Cessna Citation flight testing. The subscript e defines the error term, e. g. $\gamma_e = gamma_{\textbf{com}} - \gamma$. When comparing Fig. 3 to the initial designs in [1], it can be seen that the speed priority switch, $i_{V,\text{prio}}$, has been added. This enables the disconnection of the FPA error feedback from the pitch attitude command channel if necessary. The switch is triggered in case of thrust saturation or reaching the speed envelope boundary by the pseudo-control hedging logic (not depicted in Fig. 3). Furthermore, the gain K_f is set to a value of 1 for the flight tests with the Cessna Citation to test equally for speed and altitude tracking. For the final implementation on the HALE aircraft, however, the value will be set to 2 in order to emphasize the speed priority.

The proportional and integral gains for the specific energy rate in (Eq. (3)) and specific energy distribution (Eq. (6)) are tuned via an optimization process as described in [3]. The optimization targets are a bandwidth of 25% of the inner loop bandwidth, together with satisfactory gain and phase margins, as well as adequate disturbance rejection.

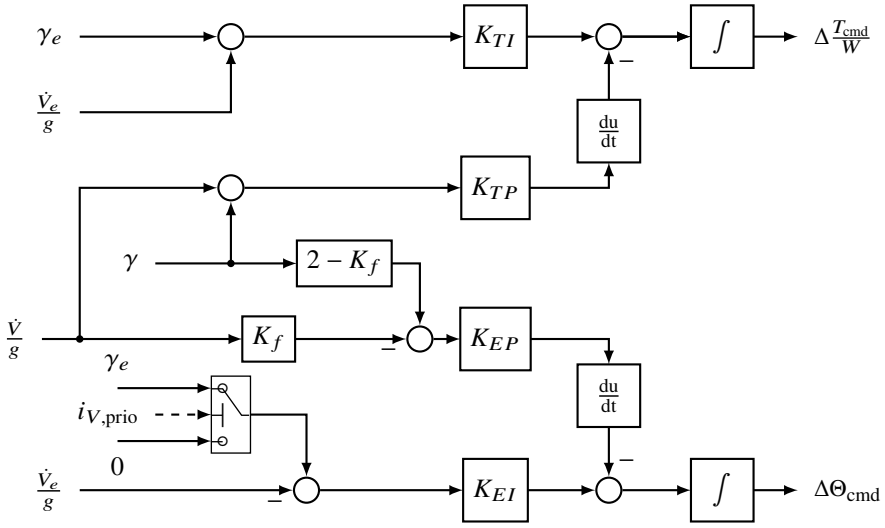

Fig. 3 TECS controller architecture.

C. Tuning of the TECS Autopilot

The numerical values of the gains in the TECS architecture in Fig. 3 are optimized using MATLAB. To speed up the optimization process, a longitudinal state-space model of the form

$$\begin{aligned} \dot{x} &= Ax + Bu \\ y &= Cx + Du \end{aligned} \tag{7}$$

is generated via linearization of the non-linear aircraft dynamics. The state vector $x = [q,\ \alpha,\ \Theta,\ V,\ N1]^{\mathrm{T}}$ consists of the longitudinal aircraft states pitch rate, angle of attack, pitch attitude, airspeed, and engine shaft speed, respectively. The engine shaft speed was added as an additional state to the usual longitudinal model in order to avoid a direct feed-through between the power setting input δ_T and the velocity derivative output $\dot{V}$. The input vector $u = [\delta_e,\ \delta_T]^{\mathrm{T}}$ of the system consists of the elevator position and the thrust command, respectively. The output vector $y = [\Theta,\ \gamma,\ \dot{V},\ V]^{\mathrm{T}}$ contains the pitch attitude, and flight path angle γ, which is calculated from the states angle of attack and pitch attitude by the relation $\gamma = \Theta - \alpha$. Furthermore, the output $\dot{V}$ is the airspeed derivative, which is used as an input to the TECS in Fig. 3, and the airspeed V which consists simply of the state. Finally, the TECS requires altitude feedback and thus, for the altitude calculation, an additional first order model

$$h = h_0 + \int V \sin\gamma \, \mathrm{dt} \tag{8}$$

is added. The linear dynamics are augmented for the TECS tuning with an inner loop (pitch tracker) in order to stabilize the pitch dynamics and enable tracking of the TECS output $\delta\Theta$. This pitch tracker of the form

$$\delta_e = K_1 \int e_\Theta \, \mathrm{dt} + K_2 e_\Theta, \tag{9}$$

with the control error $e_\Theta = \Delta\Theta_{\mathrm{cmd}} - \Theta$, is designed by using the loop shaping method with a target bandwidth of 2 rad/s. Fig. 4 shows the frequency response of the open-loop transfer from elevator to pitch attitude (dashed, black) as well as the loop transfer function of the plant multiplied with the designed proportional-integral controller. Clearly, the bandwidth of 2 rad/s is achieved and integral behavior is ensured for reference tracking. Finally the augmented

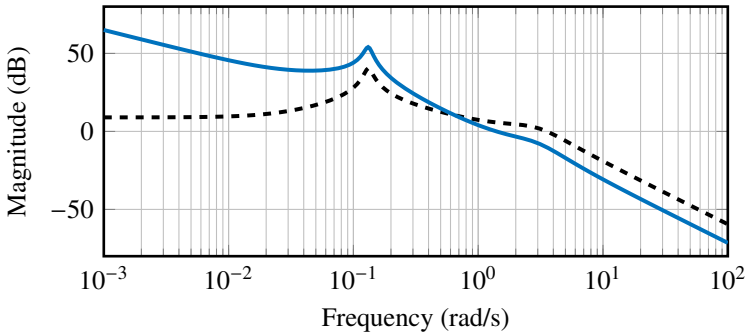

Fig. 4 Open-loop transfer function for the pitch attitude response without (- - -) and with (——) proportional-integral controller.

longitudinal dynamics together with the altitude integrator (8) facilitates the tuning of all the TECS gains (listed in Table 1) for which the Multi-Objective Parameter Synthesis (MOPS) tool described in [16–18] is used. The optimization is set up as min/max optimization problem minimizing the criteria f_i with respect to the constraints g_j as well as individual upper and lower bound, $K_{\mathrm{min},l}$ and $K_{\mathrm{max},l}$ respectively, on the optimization gains K_l, i.e.,

$$\min_{K_l} \max_{i,k} \quad f_i^{(k)}(K_l)) \tag{10}$$

$$\text{s.t.} \quad \max_{j,k} \ g_j^{(k)}(K_l) < 1 \tag{11}$$

$$K_{\mathrm{min},l} < K_l < K_{\mathrm{max},l} \tag{12}$$

Table 1 TECS gains.

Parameter	min	max	tuned?	value
K_{TI}	0	3	y	0.30
K_{TP}	0	3	y	1.06
K_{EI}	0	3	y	0.32
K_{EP}	0	3	y	1.05
K_f	0	3	n	1
K_V	0	3	n	0.05
K_H	0	3	n	0.05

Table 2 Controller Requirements.

Parameter	type	required	achieved
Rise time H [s]	min	30	31
Rise time V_{tas} [s]	min	30	39
Overshoot H [-]	min	0.001	0.004
Overshoot V_{TAS} [-]	min	0.01	0.003
Max. cross coupling (xc) [-]	min	1	1.3
Control activity $\delta\Theta_{com}$ [-]	min	3	2.7
gain margin [dB]	constraint	[4, 6]	5.7
phase margin [deg]	constraint	[30, 45]	35

For the optimization, the tuning requirements as listed in Table 2 are defined: rise time and overshoot for both, altitude- and airspeed-tracking, cross-coupling between the two variables, control activity, as well as gain and phase margins. For the calculation of the gain and phase margins, standard multi input multi output (MIMO) disk margins are used since the TECS together with the pitch tracker is a MIMO control problem with its two channels in altitude and airspeed as inputs and two control variables thrust and elevator deflection as outputs. As described in Table 2 all requirements but the stability margins are minimized throughout the optimization, while the margins are realized as design constraints. Note that the phrasing $[m, n]$ for the margins reads as follows: a values greater than n corresponds to the constraint value set to zero (completely fulfilled, not influencing the overall optimization). In the range between m and n, the value is linearly scaled between 0 and 1, and for values smaller than m, the value is larger than one and thus driving the optimization since the constraint is not fulfilled.

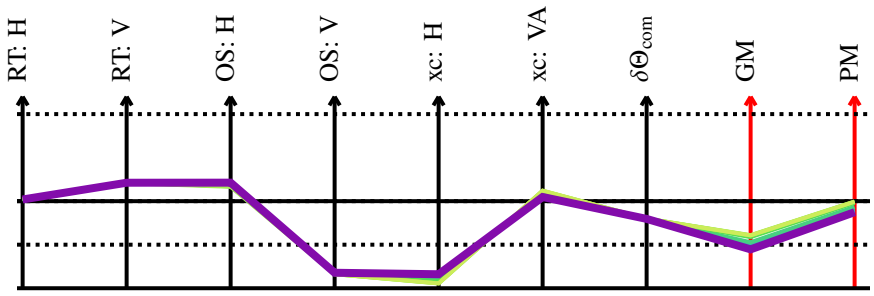

Fig. 5 Visualization of tuning goals (to be minimized: black) and constraints (red) for the optimization.

The tuning results are depicted in Fig. 5. It shows the values of the minimization criteria (black) and the constraints (red) for each evaluation. The selected, best evaluation is highlighted (—). Both figures indicate that the starting values were chosen are close to the final solution. This is due to the fact, that [1] provides already quite good estimates to which value to set the controller gains. The solid horizontal line shows the target value of 1 for all normalized criteria. It can be seen that after a total of 31 iterations the cross-coupling and overshoot criteria for the altitude tracking step did slightly improve.

III. Flight Experiments

This section provides a comprehensive overview of the Cessna Citation research aircraft utilized for flight testing, in conjunction with a detailed introduction of the software architecture employed during the flight tests. Moreover, it expounds on the rationale behind the maneuver selection and discusses the analysis of flight test data.

A. Test aircraft and control system

The Cessna Citation PH-LAB (see Fig. 6), jointly operated by TU Delft and the Dutch Aerospace Center (NLR), serves as multi-functional research platform. The aircraft is certified according to CS25 specifications for large airplanes and equipped with a conventional, fully reversible flight control system providing a fix-geared link between the pilot's controls and the aircraft's control surfaces. Moreover, an autopilot system, possessing authority over the critical primary flight controls (elevator, aileron, and rudder) is incorporated. The test aircraft has an experimental fly-by-wire (FBW) system [19], which uses the autopilot servos as control actuators. This setup has been thoroughly tested and is also certified under CS 25 [20]. A flight test instrumentation system [21], including further sensors (angle of attack, sideslip, angular acceleration, etc.) is available for data acquisition and logging. More details on the hardware setup can be found in Refs [8, 19, 21].

Fig. 6 Cessna Model 550 Citation II Research Aircraft "PH-LAB". [22]

B. Experiment Architecture

In Fig. 7, the schematic diagram of the TECS autopilot implementation onboard the Citation aircraft is depicted. The input signals, produced either by the pilot or automatically, are the desired FPA γ_{cmd} and the airspeed V_{cmd}. Instead of the FPA, it is possible to select the desired altitude h_{cmd}, which is then transferred into a flight path angle command via

$$\gamma_{\text{cmd}} = \frac{K_H}{V_{\text{tas}}}(h_{\text{cmd}} - h). \tag{13}$$

The same principle is applied for the computation of the acceleration command $\dot{V}_{\text{cmd}}$, which is computed from the airspeed command V_{cmd} and the actual airspeed:

$$\dot{V}_{\text{cmd}} = K_V(V_{\text{cmd}} - V). \tag{14}$$

The gains k_H and k_V have fixed values (i.e., they are not tuned together with the TECS gains) and are set to 0.05, as shown in Table 1. As illustrated in Fig. 7, these command inputs $\dot{V}_{\text{cmd}}$ and γ_{cmd}, as well as the respective feedback

signals, enter the TECS core block depicted in Fig. 3) . The outputs of the TECS are the commanded pitch attitude $\Delta\Theta_{\text{cmd}}$, which is transferred to the inner loop controller, and the desired thrust-to-weight ratio $\Delta T/(mg)_{\text{cmd}}$. This thrust-to-weight ratio is transformed into a throttle setting demand, $\delta_{T,\text{cmd}}$, using the aircraft's mass and an inverse engine model as depicted on the right-hand side of Fig. 7. Since the Cessna Citation used for the flight experiment does not have an auto-throttle, the throttle demand, $\delta_{T,\text{cmd}}$ is shown to the pilot on a display. The display unit coincides with the aircraft's power target and is the engine's main spool rotational speed N1 (in percent). This generally coincides quite well with the amount of thrust produced by the engine. The pilot, who acts as a substitute for the auto-throttle system, however, adds additional dynamics that need to be taken into account explicitly when tuning the autopilot. Finally, the resulting throttle setting δ_T is transferred to the engine. This engine throttle setting and the pitch attitude demand $\Delta\Theta_{\text{cmd}}$, which exit the block diagram in Fig. 7, can also be found in Fig. 2. Therein, these signals exit the autopilot block and while the pitch attitude demand enter the inner loop controller, the throttle setting δ_T is processed to the the aircraft model G directly.

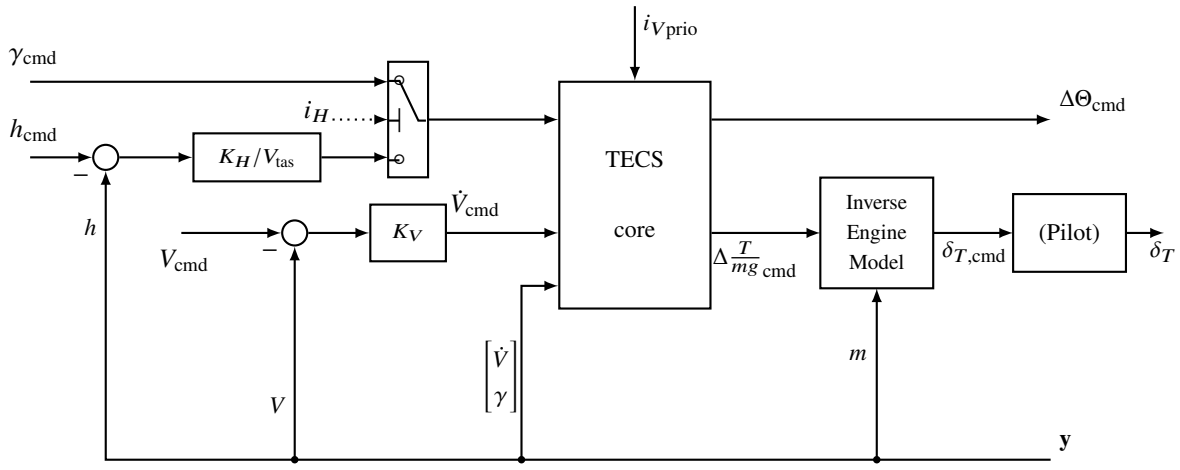

Fig. 7 Cessna Citation Autopilot architecture.

The only difference in implementation of the outer loop architecture between the Cessna Citation flight test and the HALE aircraft simulation are the two right-hand blocks in Fig. 7: In the case of the HALE aircraft, the inverse engine model reflects the electric motors and comprises a mapping from thrust demand to motor torque setting, which additionally consists of faster dynamics compared to the Cessna Citation jet engines. Furthermore, the "Pilot" block in Fig. 7 is not present in the HALE architecture. All other blocks exist in both flight control systems and can be directly exchanged between the HALE simulation and the Cessna Citation setup. This is clearly the benefit of the flight tests presented within the following section.

For both setups, the flight control laws are implemented in MATLAB/SIMULINK and the generated program code can then be directly integrated into the flight control computer's base software. In case of the HALE aircraft, the code framework is in the C++ language. The specific C++ implementation of the flight control code is developed by the DLR Institute of Software Technology [23]. For the Cessna Citation flight testing, the TU Delft DUECA framework [24] is run onboard the Cessna Citation research aircraft. Both frameworks are able to transfer data to and from the same MATLAB/SIMULINK auto-coding result. Thus, software- and integration-wise, the performed flight testing can serve adequately as initial validation of the HALE aircraft software integration environment.

IV. Flight Test Results

During the two flight test campaigns in November 2022 and August 2023, two successful flights with an active TECS control system were performed. The following discussion will present the results of these tests:

A. Tracking Validation

In the first test, the tracking and decoupling performance is evaluated for the case of each input (FPA γ and acceleration $\dot{V}$). For this, one input, e.g., the FPA command, receives a step input while the other input stays at zero command. For the FPA, this is visualized in Fig. 8, where three different step inputs to the FPA channel are given: up,

down, up at 10, 35, and 55 s, respectively. The resulting change in the flight path angle γ is visible in Fig. 8a, showing adequate tracking performance. The control system is able to keep the acceleration, visible in Fig. 8b, as well as the TAS

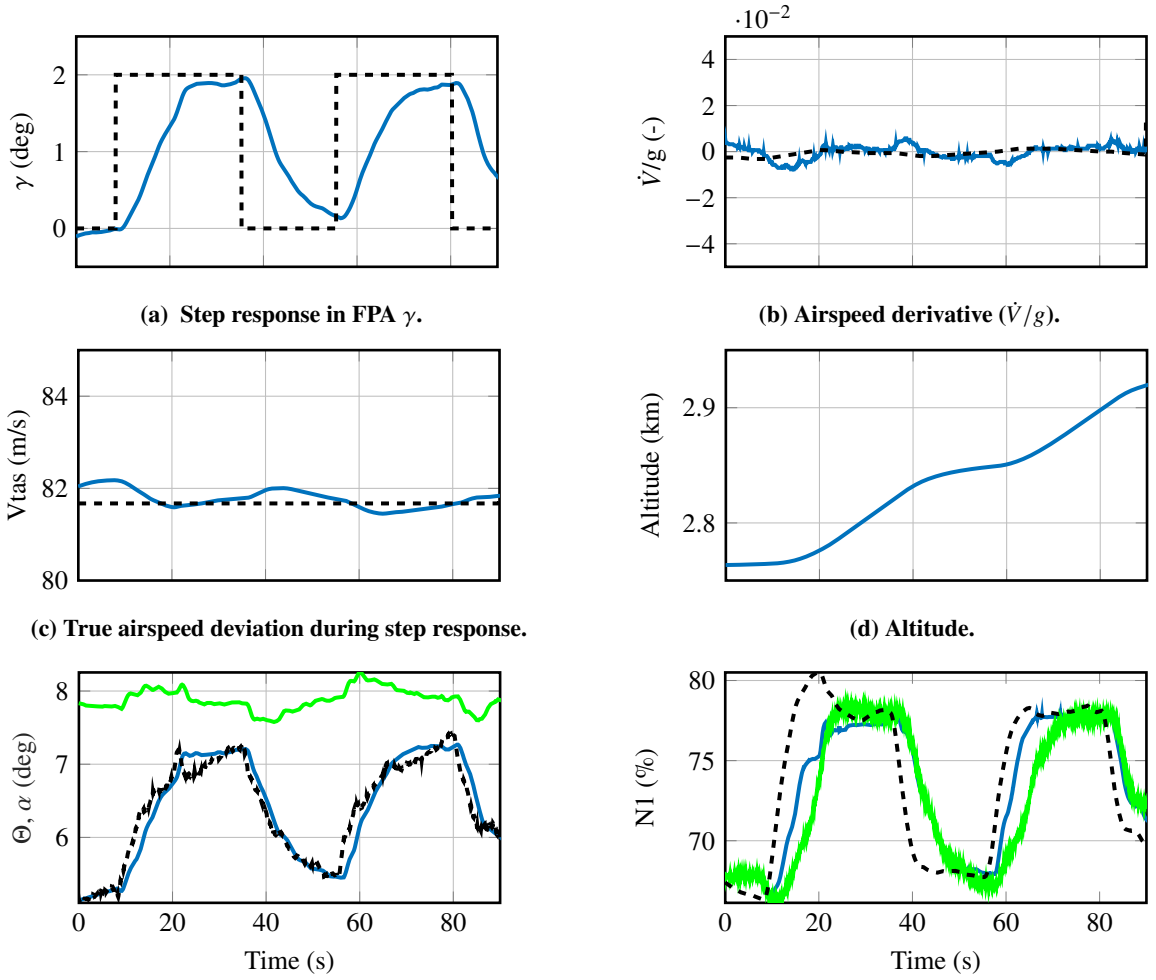

(a) Step response in FPA γ.

(b) Airspeed derivative ($\dot{V}/g$).

(c) True airspeed deviation during step response.

(d) Altitude.

(e) Pitch attitude (——), command (- - -) and angle of attack (——).

(f) Thrust command (- - -), engine thrust left (——) and right (——).

Fig. 8 Flight test data during step inputs on the FPA γ.

deviation (Fig. 8c) from the target velocity, close to zero. The resulting altitude changes are depicted in Fig. 8d. The smooth response in pitch attitude, FPA and altitude are crucial later for the HALE aircraft, which shall not experience large acceleration peaks to avoid excitements of the highly flexible structure. Moreover, the rejection of cross-coupling between FPA and airspeed commands is crucial for the HALE application, as the airspeed envelope is small and during altitude changes no airspeed deviation shall occur. For most of the set-point changes the pilots were able to track the N1 reference with good accuracy with a settling time of less than 15 s, visible in Fig. 8f. The reason for the noisy N1 right signal in Fig. 8f is this engine being a replacement engine with different dynamics and possibly different sensor calibration. This also explains the difference between the two engine's values during set point changes. In case of the HALE, an auto-throttle will take over this task with a similar time constant. Finally, Fig. 8e shows the pitch attitude Θ and the pitch attitude command Θ_{cmd} issued by the TECS controller. The pitch angle follows the command smoothly without large time lags.

B. Energy Exchange Maneuver

The second maneuver targets the validation of the exchange between potential and kinetic energy, which is a characteristic flight test setup for the TECS control philosophy and important to keep the HALE aircraft within its

limited flying envelope. For this test maneuver, the total energy demand stays constant, and therefore, the thrust should stay constant during the maneuver while kinetic and potential energy are exchanged. Fig. 9b visualizes the longitudinal

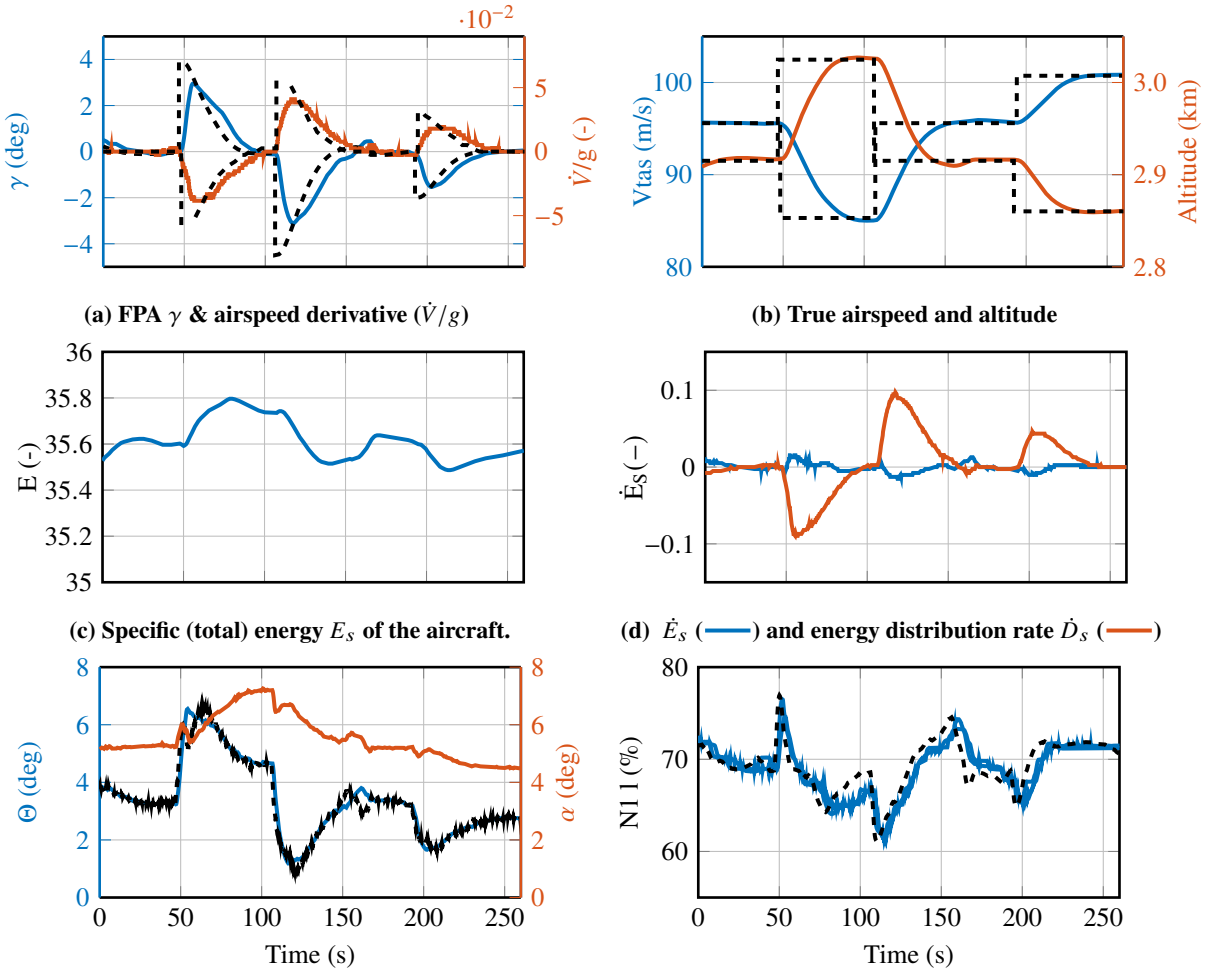

(a) FPA γ & airspeed derivative ($\dot{V}/g$)

(b) True airspeed and altitude

(c) Specific (total) energy E_s of the aircraft.

(d) $\dot{E}_s$ (——) and energy distribution rate $\dot{D}_s$ (——)

(e) Pitch attitude Θ and angle of attack α

(f) N1 command vs. actual values

Fig. 9 Flight test data of three flown energy exchange maneuvers with TECS controller active.

flight path of the aircraft during the maneuver and shows the three steps in airspeed and altitude. During the test maneuver, first, an increase in altitude in combination with a decrease in velocity of 10 m/s is initiated at t=50 s, followed by the same changes in the opposite direction at t=110 s. It can be seen that, as desired, both variables show similar time constants and settling behavior. This is a first indicator of a smooth and stable energy exchange response. Fig. 9a shows the derivatives of the specific potential and kinetic energy $\dot{D}_S$ as used in Eq. (4). Note that the scaling is chosen such that the graph visualizes the relation of the two dimensionless energy rate terms. Thus, the left scale maximum is 5 deg, while the right scale maximum for $\dot{V}/g$ is 0.09 on the y-axis (0.09 rad = 5 deg). The comparison of both graphs leads to the conclusion that the potential energy rate peaks are slightly higher for all three steps. In Fig. 9d the summation (blue) and the difference (orange) of the two curves in Fig. 9a is depicted. The sum represents the in- or decrease in total specific energy, while the difference corresponds to the exchange rate in the two energies. It can be noted that the total specific energy stays nearly constant (as the sum stays close to zero). The exchange between the specific energy rates peaks about 0.1 in both directions of the first two step inputs. The TECS command variables, pitch attitude, and thrust are depicted in Figs. 9e and 9f. Here it can be seen that the pitch attitude change, commanded for both maneuvers, is about 2.5 deg for the first two steps, while the change in thrust demand is about 7-8 % N1. While the change in thrust might seem quite large at first hand, when comparing this to the command for a pure γ step in Fig. 8 (15-20% for half the change in FPA), it becomes clear that the energy exchange already significantly reduces the change in thrust setting.

Nevertheless, as the expected outcome should have been a thrust setting change of close to zero, further investigations of the flight test data have been performed. Those led to the following conclusions:

- The maneuver was triggered in two steps due to limitations in the command interface: altitude change was triggered first, followed by the speed change with a time difference of about 0.5 s. This led to an integration in the total energy demand before the energy exchange term started to cancel out again the change in energy.
- The filtering of the FPA and $\dot{V}$ signal turned out to be insufficient, which can also be seen in the noisy pitch attitude command and thrust command signals.

Thus, both of these aspects will be taken into account for future implementations and provide an important finding of the flight test campaign. They are, however, not limiting the successful validation of the TECS autopilot system on the Cessna Citation with respect to an implementation on the HALE aircraft. This is simply because of the fact, that these two points are easily avoided when the TECS autopilot is implemented on the HALE aircraft.

C. Interpretation of Consequences for the HALE Implementation

The minor changes needed in order to adapt the TECS control laws from the HALE aircraft simulation towards the Cessna Citation flight test prove that the system is ready for use on real hardware on the HALE aircraft. The design, analysis, and code generation routines can be used with minor changes, and thus this flight test campaign provided valuable insight and confidence. In contrast to the Cessna Citation, the HALE aircraft possesses a fully automated engine command system for its electric motors. Here, the motor torque will be used as a command variable, as this is proportional to the motor current. Moreover, the electric motors have a shorter time constant than the combination of gas turbines and pilot in the Cessna Citation, and would therefore, allow a faster response of the TECS controller. On the side of the inner loop, however, a relatively slow time constant is chosen in the HALE implementation in order not to over-stress the structure and avoid the excitement of natural frequencies [3]. This counteracts the relatively quick engine dynamics, and therefore, both HALE and passenger aircraft end up with similar time constants for autopilot tracking, although resulting from different limitations.

V. Conclusions

This paper presents the design of a TECS autopilot for a HALE aircraft, which has undergone flight testing on a Cessna Citation research aircraft. We first highlight the tuning and optimization process of the flight controller. Then, the performed flight tests maneuvers and the gathered results are discussed. Particularly, two different command scenarios have been analyzed: step responses and an energy exchange maneuver. Overall, the flight test results presented demonstrate good compliance with the expected behavior. Thus, the results suggest, that the control system design and hardware integration process utilized are feasible and the control code can be readily implemented on the HALE platform.

Acknowledgments

The authors would like to extend their gratitude to the teams at TU Delft who made the entire flight test campaign possible. Special thanks go to our esteemed partners from TU Delft, who provided both the flight test framework and their invaluable expertise. We are particularly grateful to Menno Klaassen, Fred den Toom, Olaf Stroosma, René van Paassen, and Ferdinand Postema. A special note of thanks must be given to our test pilots, Alexander in't Veld and Hans Mulder. Their patience, composure, and enthusiasm greatly contributed to a successful and safe flight test experience. Additionally, we are grateful to our colleagues from the Department of Aircraft System Dynamics for their support in both the preparation and execution of the flight tests.

References

[1] Lambregts, A., "Vertical flight path and speed control autopilot design using total energy principles," *Guidance and Control Conference*, American Institute of Aeronautics and Astronautics, 1983. doi: https://doi.org/10.2514/6.1983-2239.

[2] Nikodem, F., and Bierig, A., "DLR HAP - Herausforderungen in der Entwicklung der Höhenplattform und ihrer Anwendungen," *Deutscher Luft- und Raumfahrtkongress (DLRK)*, 2020.

[3] Weiser, C., and Ossmann, D., "Baseline Flight Control System for High Altitude Long Endurance Aircraft," *AIAA SciTech 2022 Forum*, American Institute of Aeronautics and Astronautics, 2022. doi: https://doi.org/10.2514/6.2022-1390.

[4] Weiser, C., and Ossmann, D., "Fault-Tolerant Control for a High Altitude Long Endurance Aircraft," *IFAC-PapersOnLine*, Vol. 55, No. 6, 2022, pp. 724–729. doi: https://doi.org/10.1016/j.ifacol.2022.07.213, 11th IFAC Symposium on Fault Detection, Supervision and Safety for Technical Processes SAFEPROCESS 2022.

[5] Weiser, C., Ossmann, D., and Pfifer, H., "Robust Path-Following Control for High-Altitude Long-Endurance Aircraft," *Journal of Guidance, Control, and Dynamics*, 2023, pp. 1–9. doi: https://doi.org/10.2514/1.g007326.

[6] Weiser, C., Ossmann, D., Kuchar, R. O., Müller, R., Milz, D. M., and Looye, G., "Flight Testing a Linear Parameter Varying Control Law on a Passenger Aircraft," *AIAA Scitech 2020 Forum*, American Institute of Aeronautics and Astronautics, 2020. doi: https://doi.org/10.2514/6.2020-1618.

[7] Weiser, C., Ossmann, D., and Looye, G., "Design and flight test of a linear parameter varying flight controller," *CEAS Aeronautical Journal*, Vol. 11, No. 4, 2020, pp. 955–969. doi: https://doi.org/10.1007/s13272-020-00461-y.

[8] Grondman, F., Looye, G., Kuchar, R. O., Chu, Q. P., and Van Kampen, E.-J., "Design and Flight Testing of Incremental Nonlinear Dynamic Inversion-based Control Laws for a Passenger Aircraft," *2018 AIAA Guidance, Navigation, and Control Conference*, American Institute of Aeronautics and Astronautics, 2018. doi: https://doi.org/10.2514/6.2018-0385.

[9] Keijzer, T., Looye, G., Chu, Q. P., and Kampen, E.-J. V., "Design and Flight Testing of Incremental Backstepping based Control Laws with Angular Accelerometer Feedback," *AIAA Scitech 2019 Forum*, American Institute of Aeronautics and Astronautics, 2019. doi: https://doi.org/10.2514/6.2019-0129.

[10] Pollack, T., Looye, G., and der Linden, F. V., "Design and flight testing of flight control laws integrating incremental nonlinear dynamic inversion and servo current control," *AIAA Scitech 2019 Forum*, American Institute of Aeronautics and Astronautics, 2019. doi: https://doi.org/10.2514/6.2019-0130.

[11] Lambregts, A. A., "TECS Generalized Airplane Control System Design – An Update," *Advances in Aerospace Guidance, Navigation and Control*, Springer Berlin Heidelberg, 2013, pp. 503–534.

[12] Milz, D., Looye, G., and May, M., "Dynamic Inversion: An Incrementally Evolving Methodology for Flight Control Design," , 2023. To be published.

[13] van der Linden, C. A. A. M., *Dasmat-Delft University Aircraft Simulation Model and Analysis Tool: A Matlab, Simulink Environment for Flight Dynamics and Control Analysis (Series 03 - Control and Stimulation , No 03)*, Delft Univ Pr, 1998.

[14] Bruce, K. R., Kelly, J. R., and Person, L. J., "NASA B737 flight test results of the Total Energy Control System," *AIAA Astrodynamics Conference*, 1986. doi: https://doi.org/10.2514/6.1986-2143.

[15] Kastner, N., and Looye, G., "Generic TECS based autopilot for an electric high altitude solar powered aircraft," *Proceedings of the EuroGNC 2013, 2nd CEAS Specialist Conference onGuidance, Navigation & Control*, 2013, pp. 1324–1343.

[16] Joos, H.-D., "Multi-Objective Parameter Synthesis (MOPS)," *Robust Flight Control, Lecture Notes in Control and Information Sciences 224, J.-F. Magni, S. Bennani and J. Terlouw (EDS), London*, Springer, 1997, pp. 199–217.

[17] Joos, H.-D., Bals, J., Looye, G., Schnepper, K., and Varga, A., "A multi-objective optimisation-based software environment for control systems design," *IEEE International Conference on Control Applications and International Symposium on Computer Aided Control Systems Design*, 2002, pp. 7–14.

[18] Looye, G., and Joos, H.-D., "Design of Autoland Controller Functions with Multiobjective Optimization," *Journal of Guidance, Control, and Dynamics*, Vol. 29, No. 2, 2006, pp. 475–484. doi: https://doi.org/10.2514/1.8797.

[19] Zaal, P., Pool, D., in 't Veld, A., Postema, F., Mulder, M., van Paassen, M., and Mulder, J., "Design and Certification of a Fly-by-Wire System with Minimal Impact on the Original Flight Controls," *AIAA Guidance, Navigation, and Control Conference*, American Institute of Aeronautics and Astronautics, 2009. doi: https://doi.org/10.2514/6.2009-5985.

[20] European Aviation Safety Agency, *Certification Specifications and Acceptable Means of Compliance for Large Aeroplanes CS-25*, 2018.

[21] Muis, A., Oliveira, J., and Mulder, J. A., "Development of a flexible flight test instrumentation system," *17th SFTE (EC) Symposium*, 2006.

[22] Wilson, A., "Cessna Citation II PH-LAB," , 2019-05-24. URL `https://commons.wikimedia.org/wiki/File:Cessna_Citation_II_'PH-LAB'_(49318869141).jpg`.

[23] Sommer, J., "Commit, Release, Package: Automation in the development process for the ReFEx GNC System," *15th Annual Workshop on Spacecraft Flight Software*, 2022.

[24] van Paassen, M., Stroosma, O., and Delatour, J., "DUECA - Data-driven activation in distributed real-time computation," *Modeling and Simulation Technologies Conference*, American Institute of Aeronautics and Astronautics, 2000. doi: https://doi.org/10.2514/6.2000-4503.